Lab on a Chip

PAPER

View Article Online
View Journal | View Issue

Cite this: *Lab Chip*, 2026, **26**, 2266

Dissociable perfusion chip (DPC): perfusable microfluidic chip for single-cell screening of anti-cancer drugs in live glioblastoma explants

Darragh G. Kennedy,†[a] Wenting Zhao,†[b] Terry L. Chern,[a] Michael Yang,[a] Nicolas Acosta,[a] Siddarth Arumugam,[a] Pavan Upadhyayula,[c] Julia Furnari,[c] Athanassios Dovas,[d] Jeffrey N. Bruce,[c] Peter Canoll,[cd] Samuel K. Sia *[a] and Peter A. Sims*[be]

New approaches are needed to screen anti-cancer drugs that can target specific subpopulations of tumor cells. This study presents a microfluidic chip that enables parallel culture and drug perturbation of five thick tissue slices from human GBM resections, and removes the slices non-destructively for downstream single-cell RNA sequencing (scRNA-seq). Importantly, in contrast to methods relying on chemical attachment of tissue to chip, mechanical clamping of layers allows for positive-pressure perfusion of 3D slices and nondisruptive dissociation of tissue slices from the microfluidic chip. We ran the dissociable perfusion chip (DPC) on slice cultures freshly resected from human glioblastoma (within 1 h of surgery), one of the deadliest forms of malignant brain tumor which exhibits profound intra-tumoral heterogeneity that is challenging to recapitulate even with patient-derived models. DPC maintained similar fluidic conditions between channels and high cell viability in slices, and enabled downstream scRNA-seq to confirm that a topoisomerase inhibitor targets a subpopulation of proliferating tumor cells. Tissues run on DPC showed oxidative stress levels more similar to uncultured GBM slices compared to Transwell culture, as demonstrated by scRNA-seq, fluorometric assessment on a separate human patient sample, and assessment of long-term viability in mouse GBM samples under low and high oxygen tension. Overall, this proof-of-concept work suggests that combining DPC with off-chip scRNA-seq enables rapid, high-resolution identification of cell type-specific drug responses directly in GBM tissue from individual patients. Future work will aim to use this approach for screening of multiple drugs and further validation on additional fresh human GBM slices.

Received 30th November 2025,
Accepted 12th February 2026

DOI: 10.1039/d5lc01105a

rsc.li/loc

Introduction

Glioblastoma (GBM) is a deadly malignant brain tumor characterized by profound intra-tumoral heterogeneity, including the co-occurence of multiple cellular states with varying degrees of proliferative capacity and neural lineage resemblance.[1,2] While surgical resection is the standard-of-care at primary diagnosis, recurrence is common due to diffuse infiltration of GBM cells into the brain and resistance to chemo- and radiation therapies. Although chemotherapy can be effective against certain GBM cell populations, resistant subpopulations may persist and continue to proliferate, contributing to tumor progression.

Efforts to recapitulate patient-specific GBM heterogeneity *in vitro* have included culture of patient-derived GBM cells[3–5] and organoids.[6–8] However, cell-based models can take days to weeks to establish, necessitating a long turnaround time to receive drug screening results for use in a clinical setting. In addition, cellular expansion favors growth of proliferating cells, resulting in a loss of native-like brain and immune microenvironment, which contribute to a range of GBM phenotypes. A promising alternative approach is acute tissue slice culture, which involves culturing intact GBM tissue slices (freshly isolated from patients during surgical resection) on porous membrane inserts (Transwells) in wells for perturbation with drugs. We[1] and others[9] have shown that GBM tissue slices recapitulate the diversity of GBM phenotypes and microenvironmental components found in

[a] *Department of Biomedical Engineering, Columbia University, New York, NY 10027, USA. E-mail: ss2735@columbia.edu*
[b] *Department of Systems Biology, Columbia University Irving Medical Center, New York, NY 10032, USA. E-mail: pas2182@cumc.columbia.edu*
[c] *Department of Neurological Surgery, Columbia University Irving Medical Center, New York, NY 10032, USA*
[d] *Department of Pathology & Cell Biology, Columbia University Irving Medical Center, New York, NY 10032, USA*
[e] *Department of Biochemistry & Molecular Biophysics, Columbia University Irving Medical Center, New York, NY 10032, USA*
† Co-first authors.

the originating tumor tissue through single-cell RNA sequencing (scRNA-seq), which presents an attractive analytical readout for drug screening in slice cultures and enables deconvolution of cell type-specific drug responses. In addition, scRNA-seq of acute tissue slices facilitates rapid turnaround, raising the possibility of precision oncology in clinical treatment. However, culture throughput is low (one slice per well) and experiments, including frequent media changes, are labor-intensive (Tables S1 and S2). To increase the number of drugs for testing, multi-well devices have been developed,[10] but delivery of drugs and nutrients to tissue can be variable due to the reliance on diffusion. Perfusion has been attempted to enable automated and controlled fluid flow through an entire tissue, but such methods have relied on the use of adhesive proteins (*e.g.* laminin), are low-throughput, or otherwise have not been compatible with removal of tissue from the microfluidic chip for downstream analysis,[11,12] including single-cell analysis.

Here, we develop DPC, a microfluidic chip that provides automated and reproducible delivery of drug solution to five tumor tissue slices in one chip simultaneously; the perfusion can take place over many days without media changes. Tissue slices are placed into cavities located in channels of a multi-channel PDMS chip, which is then fastened to a membrane of fluorinated ethylene propylene (FEP) *via* screws through support pieces. The design facilitates perfusion through the entire thickness of the tissue without paths of lower resistance. This setup is easily dissociable after culture for downstream analysis. The device does not require adhesion molecules to attach tissue, such as laminin, which is commonly used to bind brain tissues for electrophysiological studies but requires harsh enzymatic or digestive protocols to remove a tissue slice. The PDMS and FEP layers facilitate equilibration of media and tissue with incubator conditions and enable gas exchange. As a proof of concept, we cultured human high-grade glioma tumor slices and performed scRNA-seq which confirmed heterogeneity was captured in each slice, and compared drug sensitivity to conventional slice culture methods.

Results

Device design and characterization

We designed the microfluidic chip to perfuse five tumor slices simultaneously while allowing for easy disassembly after culture for downstream analysis (scRNA-seq or other techniques such as whole tissue imaging) (Fig. 1). The chip allows culture of five tissue slices per chip (compared to one slice per well in Transwell). Each tissue cavity on the PDMS chip is equidistant from the inlet and receives media or drug solution at the same time (Fig. 2A). The tissue cavities fit tissue slices of 3 mm diameter and 500 μm thickness exactly, similar to dimensions used in previous studies involving GBM slice culture.[1,13–16] When slices were inserted, the cavities were designed to contain little to no dead space around the slice. To fabricate the PDMS layer, we 3D printed a patterned mold into which PDMS was poured, degassed, and baked (Fig. 2B). A FEP membrane was placed onto the patterned side of the PDMS layer, and clamped together *via* screws and support pieces to facilitate easy disassembly. This design is built on previous studies, which used screws to clamp and seal microfluidic systems.[17,18] Flow with dye confirmed no leakage (Fig. 2C).

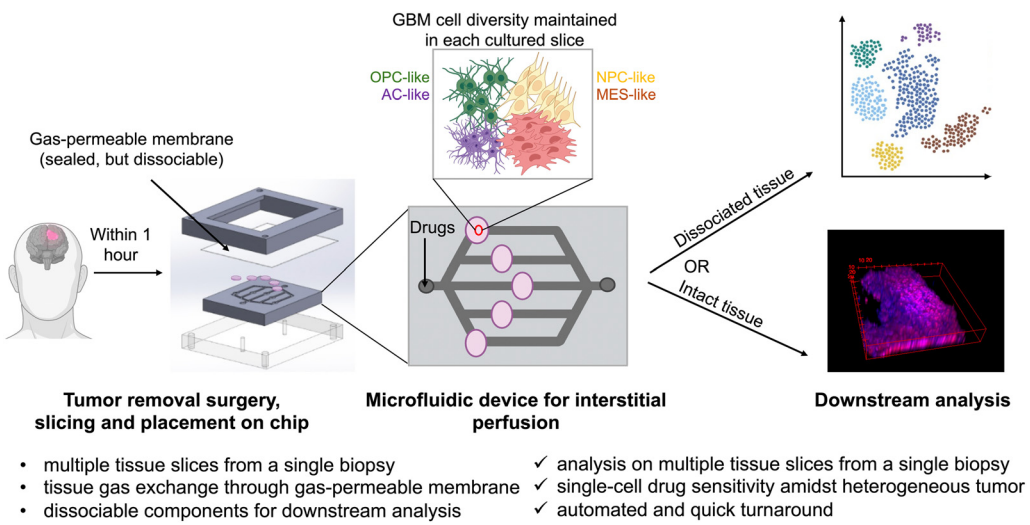

Fig. 1 Schematic diagram of the tumor perfusion system. Excess tissue from glioblastoma surgeries are taken within 1 h of surgery, and biopsy punched into slices (3 mm diameter, 500 μm thickness), and placed into cavities with the same dimensions in a PDMS chip flush at the top. A thin, gas-permeable membrane of fluorinated ethylene polymer (FEP) is placed on top, and screwing together support pieces that sandwich the PDMS–FEP mechanically seals the FEP to the PDMS. Media or drug solution can be perfused through the slices by connecting the inlet to a pre-filled syringe in a syringe pump. Each chip can culture 5 tissue slices simultaneously. After 24 h, perfusion is stopped and the system is disassembled, after which slices can be removed for whole-slice imaging or dissociated for downstream scRNA-seq. Created with http://BioRender.com.

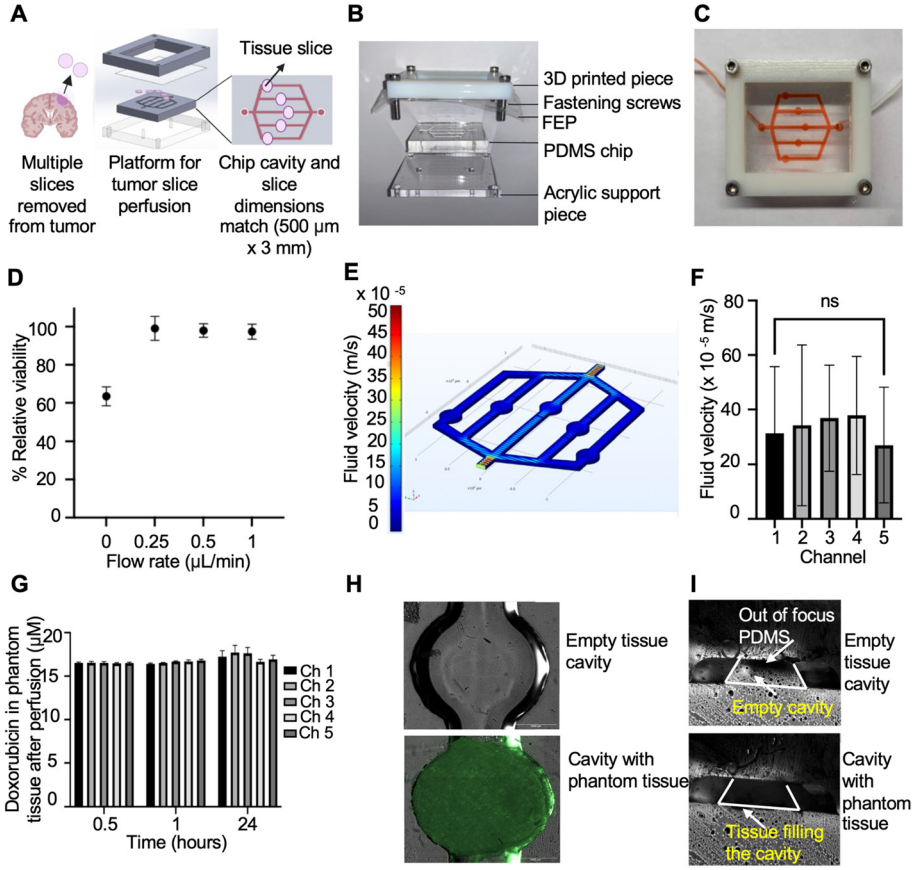

Fig. 2 Design of the DPC, and characterization of flow conditions and cell viability. A) Workflow for placing tumor slices in the DPC and design of the DPC. When a patient undergoes a routine tumor removal surgery, excess tumor tissue is sliced and within 1 h, placed on the PDMS chip. The cavity in each channel is an indent that is 3 mm in diameter and 500 μm in thickness to fit the tissue slice exactly. B) Images of the separated components of the DPC. A PDMS chip is at the center of the system and has 5 cavities for GBM tissue slices as well as one inlet for connection to a syringe and syringe pump and one outlet. After tissue slices are placed on the chip, a gas-permeable FEP layer is placed on top, and the system is sealed by mechanical clamping *via* screws in an acrylic support piece underneath the chip and a 3D printed support piece on top of the chip. There are 4 holes at the perimeter of the support pieces, which are filled with M3 screws for sealing. C) Visualization of fluid flow through the DPC once sealed, with no leaking present. Red food dye in water was perfused through the DPC at 5 μL min^{-1}. D) % viability of mouse GBM tissue slices after perfusion at various flow rates (n = 2 to 4 per flow rate), relative to Transwell-cultured tissue viability. After perfusion, the perfusion systems were disassembled, tissue slices were removed and dissociated prior to cell counting. E) COMSOL rendering of fluid velocity within the DPC when perfused at 5 μL min^{-1}. F) Average fluid velocity during perfusion in the multiplexed chip at each tissue slice cavity within the DPC, measured using the COMSOL model, n = 10 measurements per condition. Ordinary one-way ANOVA was performed. ns indicates no significant difference. G) Doxorubicin concentration in 0.6% w/v agarose brain tumor phantom slices after perfusion at 5 μL min^{-1} with 10 μM doxorubicin (n = 3). Doxorubicin concentration was measured by melting agarose slices after perfusion and quantifying doxorubicin fluorescence. H) Top-down microscopy images of one empty tissue slice cavity on the DPC (top) and loaded with a mouse dorsal skin tissue slice that was stained with FITC (bottom). Scale bar is 1 mm. I) Microscopy images of one tumor slice cavity on the DPC without tissue (top) and loaded with a mouse dorsal skin tissue slice (bottom). All data are mean ± standard deviation. Created with http://BioRender.com.

We first designed a single-channel DPC to optimize flow rates. Mouse brain tumor slices were placed on several single-channel perfusion systems attached to syringe pumps at various flow rates (0, 0.25, 0.5, 1 μL min^{-1}) and cultured with media for 24 h. After 24 h, the perfusion systems were disassembled, tissue slices were removed from the DPC, and dissociated using mechanical and enzymatic digestion on the gentleMACS™ dissociator, and single-cell viability was measured. Relative viability was close to 100% at 0.25, 0.5, and 1 μL min^{-1} flow rates (Fig. 2D). We proceeded with 1 μL min^{-1} for subsequent experiments, since this flow rate yields a total volume over 24 h (1.44 mL) that is similar to the amount of media involved in the conventional Transwell culture assay (1.5 mL). When scaling up to the multiplexed, five-channel DPC design, we designed the device such that all five channels received equal flow. We increased the flow rate to 5 μL min^{-1} for subsequent experiments on the five-channel system, to match the 1 μL min^{-1} flow rate optimized for the single-channel iteration.

Next, we used finite element analysis (COMSOL) to validate that fluid velocity profiles within each channel were consistent when scaling up to the multiplexed design. We developed a multiphysics simulation of fluid flow through the device, accounting for brain tissue characteristics and

device materials. As expected, fluid velocities were higher at the inlet and outlet compared to individual channels (Fig. 2E), with no significant difference in fluid velocity across different tissue cavities (Fig. 2F), after measuring point velocity at 10 locations on each of the 5 tissue cavities once flow was established (quantitative multi-point analysis is useful for assessing flow uniformity between channels, especially since at low flow rates, simulation is sensitive to numerical discretization effects.)

We next characterized the uptake of compounds into phantom tissue placed into the tissue cavities of the DPC. Doxorubicin hydrochloride is a chemotherapy drug with a molecular weight of ~580 $g\ mol^{-1}$ and is inherently fluorescent, allowing for the monitoring of tissue penetration.[19] Therefore, we chose this as a model small molecule to test drug uptake across channels of the DPC. 0.6% w/v agarose phantom slices, known to have similar material properties to brain tissue,[20] were biopsy punched to 500 μm thickness and 3 mm diameter, placed into perfusion chips, sealed, and cultured with 10 μM doxorubicin hydrochloride. After culturing for 0.5, 1, or 24 h, slices were removed from perfusion systems, melted, and sampled for fluorescence. There were no differences in drug concentration between slices, and concentrations within slices reached their maximum by 30 min culture (Fig. 2G). There was no overall difference in drug content uptake offered by perfusion or Transwell culture at any time point (Fig. S1), indicating that the DPC does hamper entry of small molecules into tissues. The maximum concentration in the agarose gels (~17 μM) was higher than the input concentration (10 μM), likely owing to doxorubicin adsorption in the agarose gel slices, a property which has been exploited for drug delivery applications.[21]

Finally, we demonstrated that the dimensions of the tissue-retaining cavity of the PDMS chip match those of the tissue slices, enabling perfusion through the tissue and sealing of the system without tissue damage. As seen in microscopy images, slices of 3 mm diameter completely fit the channel cavity in the x–y direction (>98% by cross-sectional area, Fig. 2H). Similarly, the thickness of the tissue (500 μm) matches the thickness of the tissue cavity within the PDMS channels (Fig. 2I). This design reduces paths of low resistance to fluid around the culture once filled with tissue and sealed, facilitating fluid to flow through the tissue. The absence of observed damage or cell detachment at the periphery of the tissue slices also suggests a lack of high shear stress caused by large flux around the tissue, and hence a sizable proportion of flow passing through the tissue.

DPC enables sc-RNAseq to demonstrate single-cell drug-sensitivity to etoposide

Next, we compared the performance of conventional Transwell-based slice culture to DPC for a human GBM surgical specimen, run within 1 h of tumor removal. We generated 24 tissue slices, cultured 12 of the slices in Transwells, and loaded the other 12 into the DPC. For both the Transwell and DPC slices, we treated half with vehicle (*i.e.*, DMSO) and the other half with etoposide, a small molecule chemotherapeutic and topoisomerase II poison (Fig. 3A). Topoisomerase II plays a crucial role in DNA replication during cell division, and its expression is highly specific to cycling cells in GBM, reproducibly and selectively targeting proliferating GBM cells as demonstrated across multiple patients.[1]

For human GBM tissues, clinically relevant responses to drugs are observed in 12 to 24 hours.[15,16] Here, after 24 hours of treatment, we dissociated the tissues from the DPC, and profiled each slice culture with scRNA-seq using a high-throughput microwell array platform that we have employed in numerous studies of GBM.[1,13–16] Tissue slices were predominantly comprised of glioma cells, along with subpopulations of T cells and myeloid cells (Fig. 3B). The diverse population of transformed GBM cells included cells resembling multiple neural lineages, such as oligodendrocyte progenitors (OPC-like), neuronal progenitors (NPC-like), and astrocytes (astrocyte-like), along with mesenchymal cells (Fig. 3C and D). This particular patient exhibited a bias towards a more astrocyte-like and mesenchymal phenotype, two cell states that often co-occur with high cell frequencies in GBM.[22] Most transformed cells were quiescent, with a small subpopulation (7%) of proliferating cells expressing Ki67 (Fig. 3E), a known marker of proliferation,[23] and *TOP2A*, another proliferation marker that encodes the molecular target of etoposide (Fig. 3F); treatment with etoposide reduced this subpopulation robustly for both Transwell and DPC cultures (Fig. 3G). Moreover, expression of cell cycle control genes was reduced (Fig. 3H). Thus, as confirmed by Transwell, DPC recapitulated the cellular and molecular diversity of GBM slice cultures as well as cell type-specific response to etoposide.

Interestingly, proliferating tumor cells in DPC exhibited a less robust response to etoposide (both cell frequency and cell cycle control gene expression) compared to Transwell (Fig. 3G and H). To probe the mechanism behind this difference, we performed gene set enrichment analysis (GSEA) (Fig. 3I). This large-scale analysis revealed an increase in expression of hypoxia-related genes in DPC, and an increase in expression of genes in oxidative phosphorylation in Transwell, suggesting GBM slices in DPC are less oxygenated than those in Transwell. We note the native microenvironment of GBM is hypoxic, and hypoxia and oxidative stress have been implicated in tumoral metabolism and drug resistance,[24–28] but further evidence is required to demonstrate the DPC mimics *in vivo* response better than Transwell culture.

We then analyzed the relative impact of etoposide on G1/S-phase markers in comparison to G2/M-phase markers. We found that the majority of cell cycle markers were downregulated regardless of cell cycle phase, and that the median log-fold-changes for G1/S and G2/M markers were nearly identical (both are −0.51 with no significant difference in their distributions $p = 0.64$) (Fig. 3J). Etoposide targets topoisomerase II in S-phase, leading to some cells to die in S-phase and others to arrest in G2/M and eventually enter

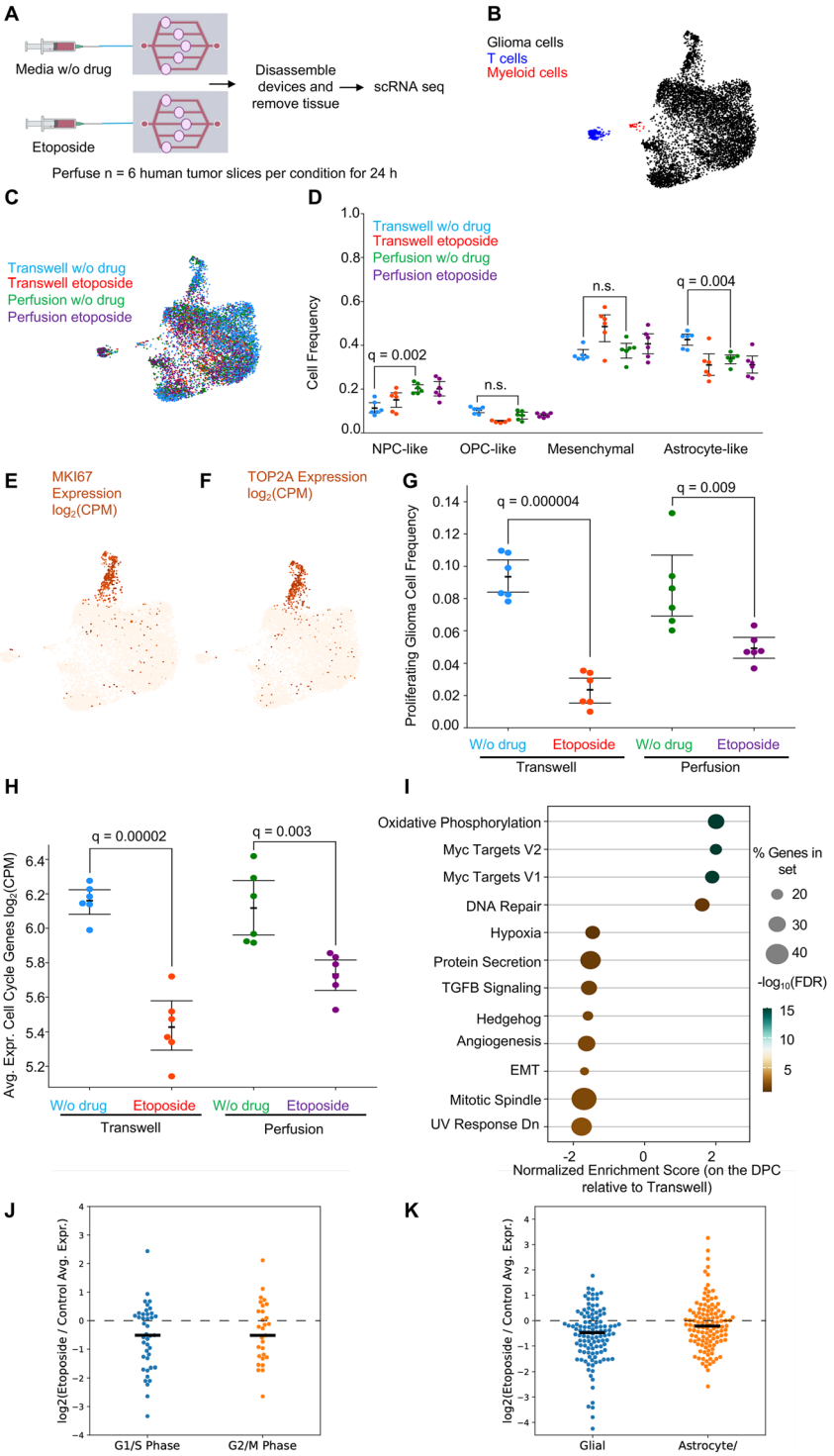

Fig. 3 Analysis of cellular heterogeneity and drug screening using DPC and downstream single-cell RNA sequencing. A) Schematic diagram of experimental workflow. 6 fresh tumor slices resected from a single human subject (3 mm diameter, 500 μm thickness) were cultured for 24 h with or without etoposide (topoisomerase II inhibitor that targets proliferating glioma cells) on Transwell or in the DPC at 5 μL min^{-1}. B) UMAP embedding of scRNA-seq profiles from slice cultures using the cell score matrix from joint scHPF analysis of the entire dataset colored by cell type. C) Same as (B) but colored by culture or perfusion condition. D) Fractional abundance of major tumor cell types in each condition. E) Same as (B) but colored by expression of Ki67. F) Same as (B) but colored by expression of TOP2A, the gene encoding DNA topoisomerase II, the target of etoposide. G) Frequency of proliferating glioma cells in each condition. H) Average expression of cell cycle genes before and after drug exposure. I) Normalized enrichment score (NES) from gene set enrichment analysis (GSEA). GSEA was performed using gene sets to analyze differentially expressed genes between Transwell-cultured and perfused tissues. Pathways that are enriched are more highly expressed in Transwell, whereas pathways that are depleted are more highly expressed in perfusion samples. J) Relative impact of etoposide on G1/S-phase markers in comparison to G2/M-phase markers. K) Relative impact of etoposide on markers of glial progenitors (left) and astrocyte/mesenchymal markers (right). All data are mean ± standard deviation. Created with http://BioRender.com.

apoptosis; hence, we expect a global impact on cycling cells regardless of phase. By contrast, when we performed the same analysis on markers of glial progenitors (which tend to have greater proliferative capacity in glioblastoma) in comparison to astrocyte/mesenchymal markers (which tend to represent quiescent cells), we saw more contrast. The median log-fold-change for glial progenitor markers was −0.5 *vs.* −0.2 for astrocyte/mesenchymal cells (p = 0.002). These findings are consistent with our previous reports showing that etoposide primarily targets proliferating cells and that glial progenitors-like tumor cells tend to be over-represented among proliferating cells (Fig. 3K).

DPC exhibits lower oxidative stress and enhances slice culture viability compared to Transwell

We further assessed oxidative stress in 3D tissue slices in DPC and Transwell[29] by culturing GBM slices freshly resected from a second human patient for 24 h. As a control, we also fixed uncultured control slices immediately upon receipt. After 24 h of culture in DPC and Transwell, the slices were also fixed. We stained slices for 8-OHdG, an indicator for oxidative DNA damage[30–34] (Fig. 4). The results showed similar and low 8-OHdG staining for native uncultured tissue taken immediately after surgery and samples cultured in DPCs. By contrast, slices cultured in Transwell showed high 8-OHdG intensity.

Because oxidative stress can adversely impact cell viability (and differences in drug screening phenotypes), we assessed long-term viability of tumor slices in DPC and Transwell under two different oxygen levels. Recognizing hypoxia can increase the viability of tumors, including GBM,[35] we cultured mouse glioma slices from a genetically engineered mouse model for up to 7 days on the DPC or on Transwell-culture systems in maintenance media, in normoxic conditions (~20% O_2) or in hypoxic conditions (5% O_2). Media were changed daily for slices in Transwell culture, while media flowed at 5 μL/min in DPC. In normoxic condition, the cells in DPC may be receiving less oxygen than those in Transwell due to lower oxygen levels in perfused culture *vs.* direct air contact (see Discussion). In normoxic conditions after 7 days, although there was no significant difference in DPC *vs.* Transwell at each individual time point, the cell viability in DPC was higher at both time points in magnitude and increasing (Fig. 5A). When culturing under hypoxic conditions (5% O_2), the viability of the Transwell slices was closer to that in DPC than under normoxic conditions (Fig. 5B).

We further developed a computational model (incorporating flow, oxygen diffusion, and cellular metabolism of oxygen) to simulate steady-state oxygen distribution in the tumor tissue cultured in DPC and Transwell (Fig. 6). A cylindrical tissue disc of the experimental geometry was modeled as a porous medium. The microfluidic model subjected the tissue to oxygen diffusing directly from the top (through the thin FEP layer) and through the PDMS laterally across the curved cylindrical surface, while advective flow from the microfluidic channel fed culture medium into the tissue from one side (Fig. 6A). The

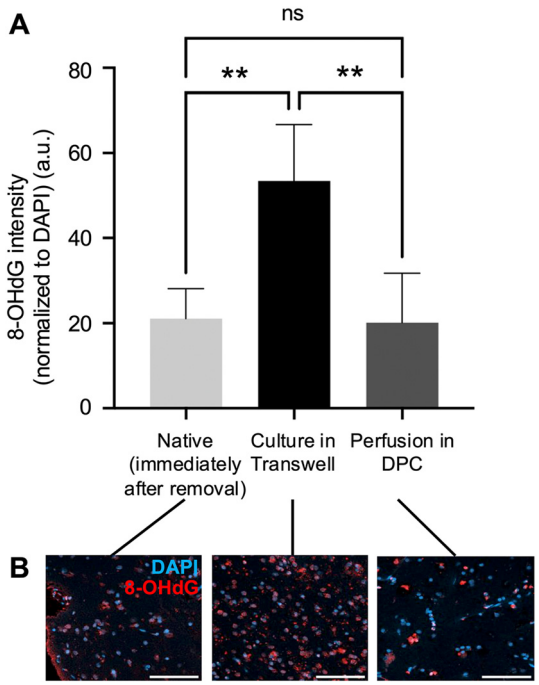

Fig. 4 Oxidative stress effects due to perfusion on human GBM tissue slices. For each culture condition, n = 4 tissue slices were tested, obtained from one human subject (different from the subject in Fig. 3). (A) Quantification of 8-hydroxy-2′-deoxyguanosine (8-OHdG) intensity in uncultured, DPC-cultured and Transwell-cultured human GBM tissue slices (n = 4 slices per condition). Immunofluorescence staining for 8-OHdG was quantified as mean fluorescence intensity for areas of the same size taken across the tumor, normalized to DAPI intensity. Ordinary one-way ANOVA with Tukey's multiple comparisons was performed. ** indicates $p < 0.01$ and ns indicates no significant difference. All data are mean ± standard deviation. (B). Representative immunofluorescence microscopy images of 8-OhdG (red) and DAPI (blue) in human GBM slices. Native slices indicate those that were fixed immediately after removal from human GBM surgery and stained. Transwell-cultured slices indicate GBM slices that were cultured on Transwell membrane inserts with standard brain slice media in 6-well plates for 24 h, followed by fixing and staining. Perfused slices indicate GBM slices perfused with standard brain slice media at 5 μL min^{-1} for 24 h, followed by fixing and staining. Scale bars 100 μm. Prior to staining, fixed slices were further sliced into 10 μm thick slices to facilitate robust imaging.

Transwell model featured an air–liquid interface, where oxygen diffused from the air from the top and sides of the cylinder, and through the media from the bottom of the cylinder's circle cross sectional area (Fig. 6A). The simulation shows a greater percent volume of cells experiencing oxygen levels under 1.5% (corresponding roughly to the oxygen levels in tumors)[54,61] in DPC, compared to Transwell, under normoxic conditions in the surrounding gas environment corresponding to that of an incubator. Under hypoxic conditions of the surrounding gas environment, the percent volumes of cells experiencing oxygen under 1.5% DPC and Transwell became more similar.

Discussion

Previously, microfluidic approaches have been explored for the culture of intact tissue slices, owing to their ability to better

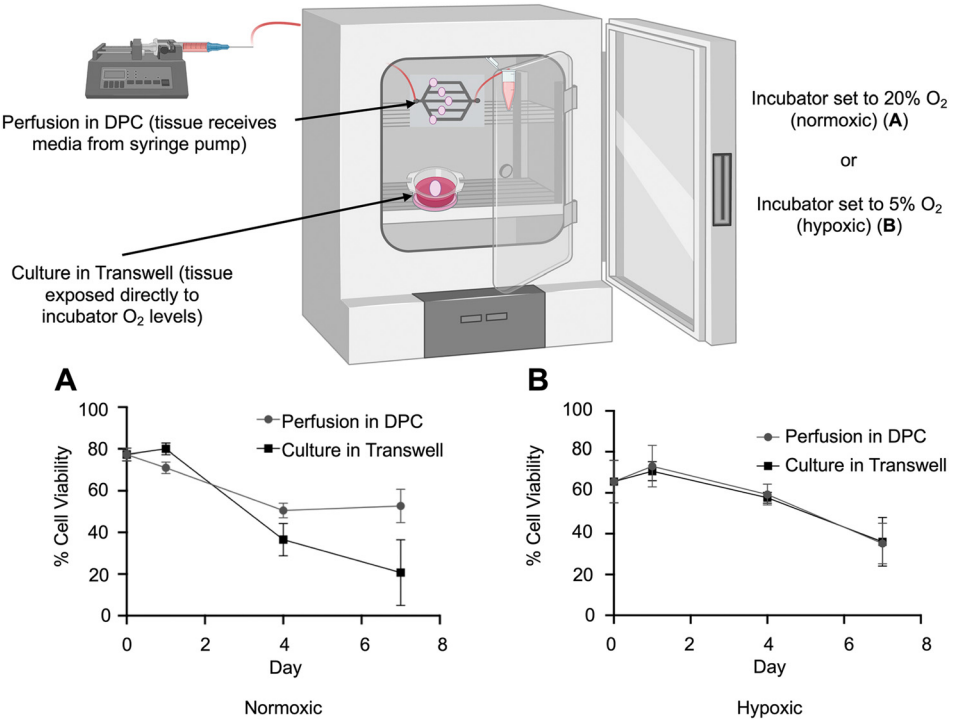

Fig. 5 Long term mouse GBM slice viability. Schematic diagram of experimental setup (top). Mouse GBM slices were cultured in the DPC or in Transwells for up to 7 days. In Transwells, mouse GBM slices are completely exposed to incubator conditions, whereas in the DPC, media is delivered from a syringe containing media to tissue *via* a syringe pump and tubing. Incubator conditions were set to normoxic or hypoxic. Quantification of tissue viability expressed as% cell viability on day 0 (fresh tissue) or after culture in DPC or Transwells at day 1, 4 and 7 (n = 2 to 8) in (A) normoxic conditions (~20% O_2) and in (B) hypoxic conditions (5% O_2). Slices were dissociated before measurement of viability. All data are mean ± standard deviation. Unpaired, two-sided Mann–Whitney U t-tests were performed in GraphPad Prism 10, showing no significant difference for each pair of cell viability values (DPC *vs.* Transwell) at each individual time point. For Transwell, there is a significant difference in normoxia *vs.* hypoxia in day 4 of Transwell, and not for other days. Created with http://BioRender.com.

support maintenance of organotypic tissues greater than 400 μm thickness.[55] Early work by Midwoud *et al.* introduced a microfluidic-based system for perifusion of precision-cut intestinal slices, and extended this to a two-compartment co-culture system enabling sequential perifusion of intestinal and liver slices for inter-organ studies.[56] Shim *et al.* also developed a multi-compartment chip to support cross-talk between tumor and lymph node slices.[57] Leveraging microfluidic platforms that trap samples in a low stress environment, Astolfi *et al.* demonstrated a proof-of-principle system for drug testing on live tumor dissections.[58] Similarly, Horowitz *et al.* developed a platform using a microfluidic circuit incorporating hydrodynamic traps to immobilize cuboidal-shaped microdissected tissues ("cuboids") for drug testing.[59] In this study, we demonstrated a DPC that cultures five thick slices of a freshly resected human tumor, enabling downstream analysis for drug sensitivity in cellular subpopulations. A microfluidic chip made of conformally sealed PDMS is dissociable, but may not support positive pressure from a syringe pump; the fluidic resistance, which the microfluidic chip must support, is also higher in 3D slices. Mechanical clamping allowed for controllable perfusion through 3D tissues as well as dissociation of tissues from the chip to enable downstream single-cell analysis (in contrast to use of adhesive molecules such as laminin which could cause damage to tissue upon removal). Dimensions of cavities matched those of slices we routinely obtain from collaborating surgeons. The results showed the flows were controllable, with no observed low-resistance paths around the 3D slices. Fresh human and mouse GBM slices exhibited high viability and were completely intact after 24 h of culture with media or drugs, and could be analyzed by scRNA-seq.

Interestingly, large-scale GSEA analysis based on scRNA-seq revealed an increase in expression of hypoxia-related genes in DPC and an increase in expression of genes in oxidative phosphorylation in Transwell, and GBM slices cultured in the DPC exhibited low levels of oxidative stress compared to the high oxidative stress levels found in conventional Transwell culture. These results suggested GBM slices in DPC are less oxygenated than those in Transwell. A hypoxic environment was estimated by numerical simulations, and consistent with experimental measurements by GSEA (where Transwell tissue showed elevated DNA repair pathway expression, consistent with greater concentrations of reactive oxygen species and DNA damage), staining of 8-OHdG on a second freshly resected human GBM specimen, and a directional increase in cell viability for tumor slices in Transwell cultures when cultured in hypoxic conditions (consistent with previous observations that GBM cells exhibit higher viability when cultured in hypoxic conditions[35] as the native GBM tumor microenvironment is hypoxic[36]). Moreover, treatment with etoposide (which causes DNA strand breaks)

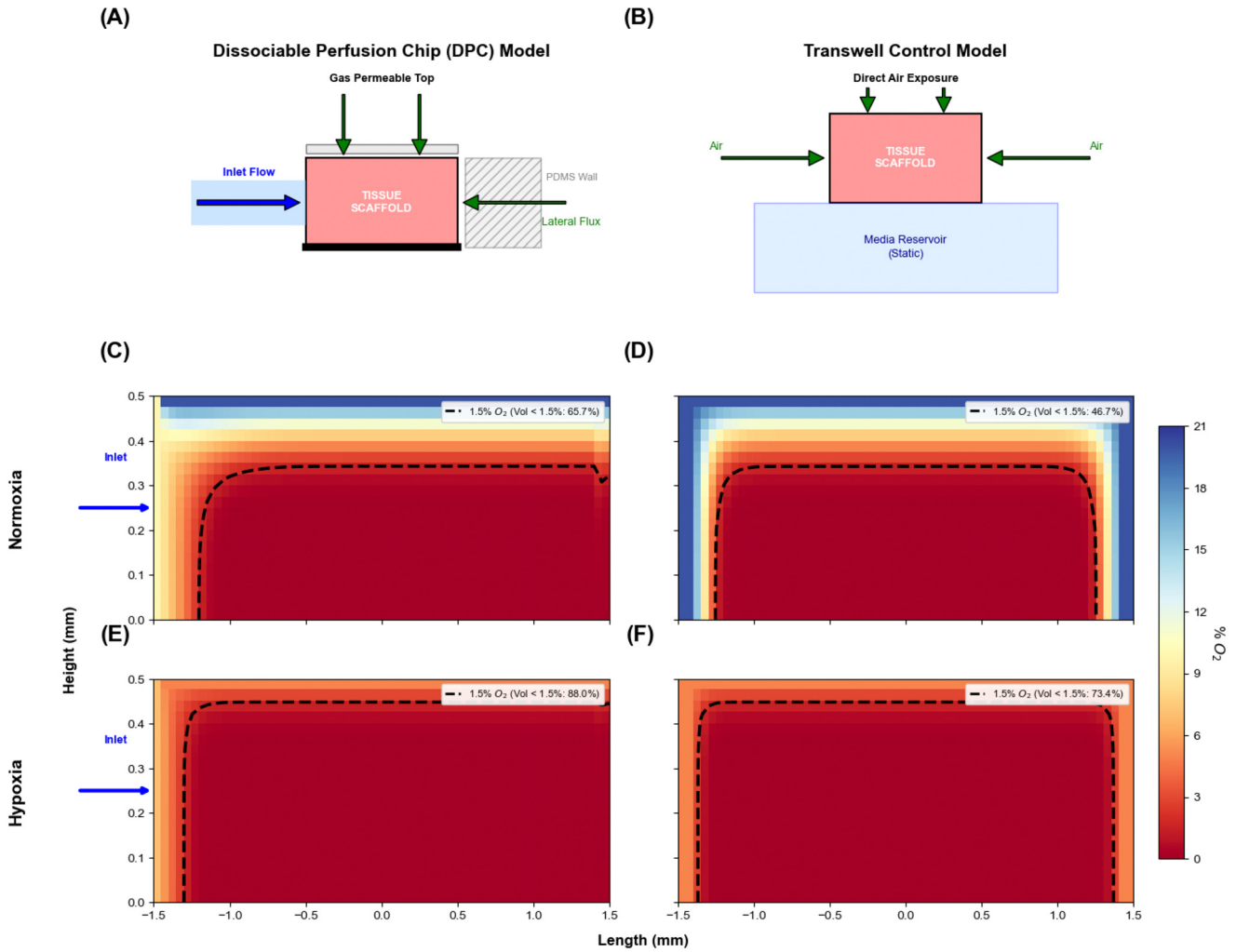

Fig. 6 Schematic diagram and results of mathematical model for steady state oxygen distribution in both the DPC and Transwell, under normoxic and hypoxic incubator conditions, mimicking the setup in Fig. 5. The top row (Fig. 6A and B) shows the model geometries and oxygen transport and consumption. The middle row (Fig. 6C and D) shows the oxygen concentration at steady state under normoxic conditions in the surrounding gas environment, and the bottom row (Fig. 6E and F) under hypoxic conditions. The middle and bottom rows illustrate side views of the simulation, cut at the centerline, with the black dotted line denoting the cutoff of 1.5% oxygen (approximating that of moderate hypoxia[54,61]), illustrating volumes of cells in the tissue experiencing oxygen levels below 1.5%. The DPC models showed greater volumes of cells below 1.5% oxygen in both normoxic and hypoxic gas environments; the greater hypoxic volume was found on the side of the cylindrical surface away from the inlet, and at deeper levels of the tissue from the top, reflecting, respectively, oxygen being consumed by cells as media flows through the tissue and less diffusion of oxygen from the gas environment vertically down deeper into the tissue.

produced an exaggerated response in the subpopulation of proliferating human GBM cells in Transwell, consistent with higher oxidative stress compounding the cumulative DNA damage.[37,38] We note that cells in the DPC are exposed to cell culture medium in which dissolved oxygen levels may range from 10% to 20%,[39,40] whereas tissue slices in Transwell are directly exposed to air in an incubator[41] of ~20% O_2 (for normoxic conditions[42]). Hence, cells in the thick tissue slices in the DPC may be exposed to oxygen levels somewhat closer to the low levels found in GBM *in vivo* (~1 to 11%) than in Transwell culture,[42–44] but direct measurements of oxygen levels in the tissue will be needed in the future to confirm the oxygen levels.

In the future, work on the DPC would benefit from testing on additional fresh high-grade human GBM samples (beyond the two fresh human GBM samples studied here, one on drug screening, and another for oxidative stress), to strengthen the conclusions beyond the suggestive trends seen in this study, and also to represent wider heterogeneity of cellular populations. In addition, while we tested all tumor slices in this study with the same drug, more drugs and drug combinations should be tested in the future to illustrate the screening capability of the DPC. Also, future studies could involve scaling up the number of drugs, to test both commonly used GBM drugs (such as lomustine, carmustine, temozolomide and bevacizumab) and drugs which are currently in clinical trials.[45] The current protocol from slicing of tissue to placement on one DPC and exposure to a drug takes ~15 min per DPC; to test 8 anti-GBM drugs, multiple

users or automation can be used to run 8 DPCs to keep total time to 15 min (Fig. S2). Such a system could be useful for matching GBM patients to clinical trials for novel drugs under investigation.

Materials and methods

Fabrication and assembly of the DPC

The molds for the PDMS chip of the DPC were designed on Solidworks and 3D printed using VeroWhite resin on a Stratasys Objet 30 Pro. After printing, molds were washed using a basic solution and baked for at least 2 h at 65 °C. PDMS was prepared by combining prepolymer base (Sylgard 184, Dow Corning, USA) with the curing agent at a ratio of 10 : 1. After mixing by hand and centrifugation for 5 min at 3000 rpm, PDMS was poured into the mold, degassed for 1 h and then cured for 3 h at 65 °C. The cured PDMS was then removed from the mold and inlet and outlet holes were punched using a 1.25 mm biopsy punch (World Precision Instruments). The chip was then treated with oxygen plasma and autoclaved for sterilization prior to setting up the system. The resultant PDMS chip was 45 × 38 × 12 mm. Each channel of the central chip of the DPC has one slice cavity of 3 mm diameter and 500 μm thickness. The inlet, outlet and 5 tissue cavities were all designed to be 3 mm diameter. The total area of the indented channel lanes on the PDMS chip is 233.35 mm^2. The area separating lanes 1 and 2, and 4 and 5 is 76.8 mm^2, and the area separating lanes 2 and 3, and 3 and 4 is 96.35 mm^2. The chip was designed such that the distance from the inlet to the tissue cavity in each lane is ~13 mm.

We next developed an acrylic (PMMA) support piece intended to be placed under the PDMS chip, with holes laser cut to facilitate connection of tubing for the inlet and outlet, and eventual clamping of the DPC. The piece was designed on Adobe Illustrator and laser cut (Universal Laser Systems PLS6.150D). We laser cut a 60 × 50 × 5 mm rectangle into acrylic, with one circle at each of the four corners of the rectangle (3.1 mm diameter) to fit screws, and two circles towards the center of the piece (1.79 mm diameter) for tubing connection.

A piece of fluorinated ethylene polymer (FEP) of 0.001″ thickness (Holscot Europe) was then placed on top of the PDMS chip, with four holes biopsy punched at the corners of the sheet (3 mm diameter). Finally, we 3D printed a top support piece to "clamp" all components together. This top piece was designed on Solidworks and 3D printed using VeroWhite resin on a Stratasys Objet 30 Pro. The piece is 60 × 50 × 8 mm with one circle at each of the four corners (3.1 mm diameter) for screws. There is an aperture on both sides of this piece to enable exact fitting of the PDMS chip, to facilitate perfusion. The bottom face is 45 × 38 mm (same length and width as the PDMS chip), while the top face is 45 × 30 mm such that the PDMS chip does not fall out of the support piece.

Finally, the DPC is sealed by screwing the 3D printed top piece through to the FEP through to the bottom acrylic piece using M3 screws and washers (McMaster Carr). When using tissue samples, PDMS chips were plasma cleaned and autoclaved and all ancillary components were sprayed with 70% ethanol and dried prior to insertion of tissue samples. For all experiments, the inlet tubing was connected to a syringe containing media or drug solution, positively displaced by a syringe pump (GenieTouch, Kent Scientific) located outside of the incubator.

Flow rate experiments

A previous iteration of the system could retain one tissue slice in which a single-plexed PDMS chip connected to smaller components. This chip was initially used to determine ideal flow rates for maximal viability after 24 h. Tubing (Liquid Flows Tygon Tubing Coil 1/16″ OD × 0.02″ ID, Darwin Microfluidics) was connected to a syringe containing maintenance media (F12/DMEM (Gibco) supplemented with N-2 Supplement (Gibco) and 1% antibiotic–antimycotic (ThermoFisher)) and needle and positively displaced using a syringe pump (GenieTouch, Kent Scientific) located outside of the incubator, into the chip inlet. Mouse brain tumor slices (3 mm diameter, 0.5 mm height) were placed on several perfusion systems attached to syringe pumps at various flow rates (0, 0.25, 0.5, 1 μL min^{-1}) and cultured for 24 h. Tissue slices of the same dimension were also cultured for 24 hours on Transwell. Media was changed daily for slices in Transwell culture by transferring the porous membrane insert containing the tumor slice to a new well containing 1.5 mL fresh media, as well as adding 10 μL of media on top of the slice. Slices were removed and dissociated after 24 hours of culture and single-cell viability was measured using an automated cell counter (Countess 3, Invitrogen). Dissociation and cell counting is a reliable approach to measure slice viability on this timeline (~24 hours)[1,13,14,16] (with direct comparisons of dissociation/cell counting, scRNA-seq, and *in situ* mRNA hybridization for assessing viability in intact tissue[1]), compared to histopathological assessments which are appropriate for long-term studies, since cellular material originating from dead cells remains trapped in place in the intact tissue on this short timescale.

Drug uptake experiment

To confirm drug uptake owing to perfusion culture, we cultured 0.6% w/v agarose tissue slices with a solution of 10 μM doxorubicin hydrochloride (Sigma Aldrich), an inherently fluorescent anticancer compound, for up to 24 h. The molecular weight of this compound (579.98 g mol^{-1}) is similar to that of etoposide (588.557 g mol^{-1}) which was used for drug screening experiments. After 30 min, 1 h, and 24 h of culture, devices were disassembled and slices were dissociated using a tissue grinder (DWK Life Sciences). Once completely dissociated, the fluorescence intensity of the resultant solution was measured using a plate reader

(Synergy H1 hybrid multi-mode reader (BioTek, Winooski, VT)) at an excitation wavelength of 470 nm and an emission wavelength of 585 nm. The resulting data was expressed as arbitrary units (AU); and we calculated concentration using a standard curve.

Human GBM specimens

Approval was obtained from the Columbia University Irving Medical Center Institutional Review Board (IRB) before commencing the study. We strictly adhered to regulations imposed by the IRB. Informed consent was obtained from all participants. Tumor specimens were procured from surgeries at New York Presbyterian Hospital/Columbia University Irving Medical Center and tissue samples were de-identified prior to being delivered to the laboratory for processing. Acute tissue slices were generated as previously described.[1] For drug screening experiments (Fig. 3), slices from human glioblastoma, IDH wildtype, CNS WHO grade 4 (male, age range 70–74) were used. For oxidative stress staining experiments (Fig. 4), slices from human glioblastoma, IDH wildtype, CNS WHO grade 4 (female, age range 65–69) were used. In both cases, tissue was transported back to the laboratory in saline from the operating room on ice. Tissues were then sliced to 500 μm thickness and placed into artificial cerebrospinal fluid (aCSF). Once slices were ready, they were plated onto Transwell inserts first in incomplete DMEM/F12, then into complete DMEM/F12 (supplemented with N_2 and antibiotic/antimycotic). The time from excision to plating is approximately 30 min. These slices were then transported to another laboratory on ice until biopsy punched into 3 mm diameter slices and fixed (5 min), or placed into the DPC or Transwell (30 min). Two freshly resected high-grade GBM specimens were obtained.

Mouse GBM specimens

All animal procedures were approved by Columbia University Institutional Animal Care and Use Committee (IACUC) (protocol AC-AABN6552) and were carried out in accordance with the approved guidelines. Mice of both sexes (6–8 week-old) were used throughout the study. We generated gliomas by injection of 1 μL of PDGF-BB – IRES – Cre retrovirus (10^6 per mL titer) into the subcortical white matter of $P53^{fl/fl}$/$PTEN^{fl/fl}$/$Luciferase^{stop\text{-}flox}$ mice in the following coordinates (with bregma as reference): 2 mm lateral, 2 mm rostral and 2 mm deep, at a flow rate of 0.33 μL min^{-1}.[46] Tumor growth was monitored by bioluminescence imaging on an IVIS spectrum optical imaging system (Caliper) as detailed in ref. 46. When photon flux reached a radiance of 10^6–10^7 (p s^{-1} cm^{-2} sr^{-1}), animals were euthanized, the brain was excised and 500 μm – thick brain slices were obtained on a tissue chopper (McIlwain) as detailed in ref. 1. Presence of tumor in the brain sections was confirmed by *ex vivo* bioluminescence imaging. For placement onto DPCs, a 3 mm biopsy punch (World Precision Instruments) was used to gently press and excise slices of 3 mm diameter for further experiments.

Characterization of tissue placements in chip

To confirm that the tissue cavities on the PDMS chip were the same as the tissue slices we use, microscopy images were taken of the PDMS chip before and after addition of tissue slices (Leica DMI6000 B). Tissue slices were immersed in 1 mg mL^{-1} fluorescein for 30 min to enable fluorescence. To calculate the percentage fitting of tissue slices in the tissue cavities, microscopy images were uploaded to ImageJ. The areas of n = 5 empty tissue cavities and corresponding cavities with tissues included were measured, and an average % filling was calculated.

Drug screening

High WHO grade 4 glioma, IDH wild type tissue samples were biopsy punched and placed onto perfusion chips and Transwell inserts (n = 6 each) and cultured for 24 h with 2.5 μM etoposide hydrochloride dissolved in dimethyl sulfoxide (DMSO) (Sigma-Aldrich) or DMSO (drug vehicle) control. After 24 h, samples were removed from perfusion systems or Transwells, dissociated, and processed for single-cell RNA sequencing (scRNA-seq).

Dissociation of tissue and slices

Collected tissue slices were dissociated as performed previously[1] using the Adult Brain Dissociation kit (Miltenyi Biotec) on gentleMACS Octo Dissociator with Heaters (Miltenyi Biotec) according to the manufacturer's instructions.

Microwell scRNA-seq

Dissociated cells from each slice were profiled using microwell-based single-cell RNA-seq[47] as previously described.[1,48,49] A countess live-dead assay was used to measure the viability of our single-cell suspension. Briefly, libraries with unique Illumina sample indices were pooled for sequencing on (1) an Illumina NextSeq 500 with an 8-base index read, a 21-base read 1 containing cell-identifying barcodes (CB) and unique molecular identifiers (UMIs), and a 63-base read 2 containing the transcript sequence, or (2) an Illumina NovaSeq 6000 with an 8-base index read, a 26-base read 1 containing CB and UMI, and a 91-base read 2 containing the transcript sequence.

scRNA-seq data preprocessing

Raw data obtained from the Illumina NextSeq 500 was trimmed and aligned as described previously.[1,48] Briefly, for each read with a unique, strand-specific alignment to exonic sequence, we constructed an address comprised of the CB, UMI barcode, and gene identifier. Raw data obtained from the Illumina NovaSeq 6000 was first corrected for index swapping to avoid cross-talk between sample index sequences using the algorithm described by Griffiths *et al.*[50] before assigning read addresses for each sample. For samples that had been sequenced on both Illumina NextSeq 500 and NovaSeq 6000, we combined the addresses from the NextSeq 500 and the corrected addresses from the NovaSeq 6000 for

data processing as described previously.[1,48,49] Briefly, reads with the same CB, UMI, and aligned gene were collapsed and sequencing errors in the CB and UMI were corrected to generate a preliminary matrix of molecular counts for each cell.

We applied the EmptyDrops algorithm to recover true cell-identifying barcodes in the digital gene expression matrix.[51] We then removed CBs that satisfied any of the following criteria: (1) fractional alignment to the mitochondrial genome greater than 1.96 standard deviations above the mean; (2) a ratio of molecules aligning to whole gene bodies (including introns) to molecules aligning exclusively to exons greater than 1.96 standard deviations above the mean; (3) average number of reads per molecule or average number of molecules per gene >2.5 standard deviations above the mean for a given sample; or (4) more than 40% of UMI bases are T or where the average number of T-bases per UMI is at least 4.

Unsupervised clustering, differential expression, and visualization

Clustering, visualization, and identification of cluster-specific genes were performed as described previously (http://www.github.com/simslab/cluster_diffex2018).[1,48,49] We used Louvain community detection as implemented in Phenograph for unsupervised clustering with k = 20 for all k-nearest neighbor graphs. For all clustering and visualization analyses of merged datasets, we identified marker genes using the drop-out curve method described in Levitin *et al.*[49] (http://www.github.com/simslab/cluster_diffex2018) for each individual sample and took the union of the resulting marker sets to cluster and embed the merged dataset. We projected drug-treated cells onto vehicle-treated cells with UMAP in Fig. 3 as described in Szabo *et al.* and Levitin and Sims (code available at http://www.github.com/simslab/umap_projection).[52]

Cell-type-specific differential expression analysis

To identify differentially expressed genes for drug- *vs.* vehicle-treated cells, we first randomly sub-sampled the condition with a greater number of cells in each comparison to have the same number of cells as the condition with fewer cells. Next, we subsampled the count matrices for the two conditions such that they had the same average number of molecules per cell and normalized the resulting count matrix using scran.[53]

Immunohistochemistry

To investigate whether or not the perfusion system protects the tumor slices from oxidative stress compared to Transwell culture, we cultured human high-grade glioma slices for 24 h in the DPC at 5 μL min^{-1}, or on top of a porous membrane insert (0.4 μm, Millipore). For Transwell, the membrane inserts were placed into 6-well plates containing 1.5 mL of maintenance media, and added 10 μL of culture medium on top of each slice to prevent the slice surface from drying. In both cases, maintenance media was used: F12/DMEM (Gibco) supplemented with N-2 supplement (Gibco) and 1% antibiotic–antimycotic (ThermoFisher). Both the perfusion and Transwell culture setups were placed into an incubator at 37 °C and 5% CO_2. We also fixed control slices immediately upon receipt in 4% paraformaldehyde overnight at 4 °C before storing in PBS at 4 °C until staining. Immunohistochemistry was performed on 4% paraformaldehyde-fixed paraffin-embedded tissue sections (10 μm thick) to analyze 8-OHdG levels from tissue cultures grown under the indicated conditions. Tumors were sliced and embedded by the Columbia University Molecular Pathology Shared Resource (MPSR) facility. Sections were deparaffinized in xylene (3 × 5 min), followed by rehydration in 100% ethanol (2 × 5 min), 95% ethanol (2 × 5 min), and 75% ethanol (1 × 5 min). Slides were washed in water and antigen retrieval was performed in a 10 mM citrate buffer (pH 6) in a pressure cooker for 10 min. After cooling for 30 min, slides were washed in phosphate-buffered saline (PBS; pH 7.4) and blocked in 10% normal goat serum for 30 min. Primary antibody incubation was performed overnight at 4 °C using the anti-DNA/RNA damage antibody (Abcam, catalog number ab62623), and counterstained with an Alexa Fluor 568 conjugated goat-anti Mouse IgG2b secondary antibody (Thermo Fisher Scientific, catalog number A21144) and DAPI.

Microscopy

To detect changes *in situ* of 8-OHdG, images (1024 × 1024, Voxel size: 0.3120 × 0.3120 × 1 μm^3) were captured on a Zeiss LSM 900 confocal microscope using a 20×/0.8 NA Plan-Apo Air objective. Fluorophores were excited using 405 and 561 nm lasers and captured on GaAsP detectors. Images were exported to Fiji for further analysis. Immunofluorescence staining for 8-OHdG was quantified as mean fluorescence intensity for areas of the same size taken across the tumor. While nuclear density varies between conditions, and even between images in each condition (including fresh tissue), this is in line with native GBM spatial heterogeneity, including hyper- and hypocellular regions. We analyzed 8-OHdG expression by dividing integrated density owing to 8-OHdG (red) by DAPI (blue) within each image, on n = 4 images per condition, using images from various regions of the tissue slice. To this end, intensity is normalized across images, accounting for any changes in nuclear density.

Long-term viability

Mouse tumor slices (n = 3) were dissociated immediately on day 0 and single-cell viability was measured using an automated cell counter (Countess 3, Invitrogen). Mouse brain tumor slices were cultured for up to 7 days on the DPC or on Transwell-culture systems in maintenance media (F12/DMEM (Gibco) supplemented with N-2 supplement (Gibco) and 1% antibiotic–antimycotic (ThermoFisher). For "normoxic" conditions, both the DPC and Transwell-culture systems were placed in a regular incubator (set to 20% O_2). For "hypoxic" conditions, both the DPC and Transwell-culture systems were placed in an incubator set to 5% O_2 (for DPC, in the future,

placing syringe pumps and media source in the incubator may be interesting to produce even greater hypoxia). Media was changed daily for slices in Transwell culture by transferring the porous membrane insert containing the tumor slice to a new well containing 1.5 mL fresh media, as well as adding 10 μL of media on top of the slice. Media was constantly flowing at 5 μL min^{-1} in the DPC. Slices were removed and dissociated after 1, 4 and 7 days of culture and single-cell viability was measured using an automated cell counter (Countess 3, Invitrogen). Again, dissociation and cell counting is a reliable approach to measure slice viability on this timeline since cellular material originating from dead cells remains trapped in place in the intact tissue on this timescale.

Computational model of steady-state oxygen levels in DPC and Transwell

To characterize the oxygen microenvironment within the tissue samples, we developed a custom 3D finite difference model to simulate the reaction–diffusion–advection physics for the microfluidic DPC chip and Transwell (this combination of physics is not found in standard packages; our source code is available upon request). The mathematical model was implemented in Python (Python 3.12.10) using a custom finite difference solver. The domain was discretized into a structured Cartesian grid (60 × 60 × 20 voxels), which yielded a spatial resolution of 50 micrometers in the *xy*-plane and 25 micrometers in the *z*-direction. The system was solved using an explicit forward-Euler time-stepping scheme (dt = 5 ms) for 5000 time steps, once a steady state condition was reached (convergence criterion of <0.1% change over 100 steps). The simulation represented the geometry of the experimental tumor tissue geometry (cylindrical tissue disc of d = 3.0 mm, h = 0.5 mm) modeled as a porous medium.

Oxygen transport was modeled accounting for diffusion, advective flow from the inlet, and metabolic consumption by the tumor cells. Key parameters were chosen based on literature values for tumor microenvironment:

- Porosity (phi): porosity was set to the porosity of brain tissue, 0.2.[60]
- Diffusivity (D_tissue): oxygen diffusivity in the tissue was set to 1.5 × 10^{-3} mm^2 s^{-1}, reflecting the nature of the tumor tissue.[62]
- Metabolic consumption (V_max): cellular oxygen consumption was modeled using Michaelis–Menten kinetics with a maximum consumption rate (V_{max}) of 13.0 mmHg s^{-1} and a Michaelis constant (K_m) of 2.5 mmHg.[63,64] The V_max value was calibrated to bound the upper limits of experimentally observed viability as shown in Fig. 5.

We simulated two physical configurations for DPC and Transwell:

○ DPC: the geometry (Fig. 6A) accounts for oxygen diffusion through the gas-permeable PDMS side walls, as well as diffusion of oxygen directly from the gas environment through a cross-sectional top circle area. Diffusion through PDMS was modeled as a resistive flux boundary condition (k_transfer = 0.15) driven by the gradient between the tissue edge and the incubator environment. Advective flow rates corresponded to experimental values: 5 μL min^{-1} for the chip (with each of the 5 lanes around ~1 μL min^{-1}).

○ Transwell: the geometry (Fig. 6B) simulates a static (*i.e.* with no advective flow) air–liquid interface culture. The top and side surfaces were exposed directly to the gas environment.

○ Environmental conditions: simulations were performed for both normoxic and hypoxic incubator conditions. In the normoxic condition, inlet air and incubator air were set to 76 mmHg (10% oxygen) and 152 mmHg (20% oxygen) respectively. In the hypoxic condition, to match the experimental hypoxic chamber, the inlet air and incubator air were set to 53.2 mmHg (7% oxygen) and 38 mmHg (5% oxygen) respectively. For DPC, we modeled the inlet oxygen concentration in normoxic environment to be 10% (an estimate of dissolved oxygen levels, see Discussion), and in hypoxic environment to be 7% to reflect partial adjustment to the 5% oxygen as the culture medium passed through the incubator (within Tygon tubing, which is gas-permeable) before flowing through the tissue.

Statistics and number of mouse and human GBM specimens tested

All statistical analysis was performed using GraphPad Prism 10. Data shown are mean ± standard deviation unless otherwise noted. Mouse tumor slices were used for viability testing (Fig. 2D and 5). For the initial flow rate *vs.* viability study, mouse tumor slices were obtained and n = 2–4 slices were cultured on both the DPC and Transwell. For the long-term viability study, mouse tumor slices were obtained and n = 2–8 slices used per condition (day 0, and days 1, 4, 7 for both DPC and Transwell). For the drug screening experiment (Fig. 3), slices were obtained from one human high WHO grade 4 glioma, IDH wild type case. N = 6 slices (3 mm diameter, 500 μm thickness) were cultured for each of the four conditions (DPC etoposide, DPC without, Transwell etoposide, Transwell without drug). For oxidative stress staining (Fig. 4), slices were obtained from a second human glioma, with n = 4 slices tested per condition (uncultured, DPC, and Transwell). For future validation of this platform for drug screening, it will be necessary to test more than two human specimens. Enough tissue slices must be derived from one patient to test the range of targeted conditions (4 in this study, with DPC and Transwell with and without drug, but more conditions with multiple drugs), and the surgery must be coordinated with the running of the chip within hours.

Conflicts of interest

There are no conflicts to declare.

Data availability

The data supporting this article have been included as part of the main text and within supplementary information (SI). In addition, please refer to the methods section for the various detailed methods used to analyze the data.

Supplementary information is available. See DOI: https://doi.org/10.1039/d5lc01105a

Acknowledgements

These studies used the Confocal and Specialized Microscopy Shared Resource of the Herbert Irving Comprehensive Cancer Center at Columbia University, funded in part through the NIH/NCI Cancer Center Support Grant P30CA013696. This study was also supported by Columbia University Pilot Project HICCC Grant UR011736.

References

1 W. Zhao, A. Dovas, E. F. Spinazzi, H. M. Levitin, M. A. Banu and P. Upadhyayula, *et al.*, Deconvolution of cell type-specific drug responses in human tumor tissue with single-cell RNA-seq, *Genome Med.*, 2021, **13**(1), 82.

2 X. Sun and Q. Yu, Intra-tumor heterogeneity of cancer cells and its implications for cancer treatment, *Acta Pharmacol. Sin.*, 2015, **36**(10), 1219–1227.

3 H.-G. Yi, Y. H. Jeong, Y. Kim, Y.-J. Choi, H. E. Moon and S. H. Park, *et al.*, A bioprinted human-glioblastoma-on-a-chip for the identification of patient-specific responses to chemoradiotherapy, *Nat. Biomed. Eng.*, 2019, **3**(7), 509–519.

4 E. Stavrakaki, W. B. L. van den Bossche, L. B. Vogelezang, C. Teodosio, D. M. Mustafa and J. J. M. van Dongen, *et al.*, An autologous ex vivo model for exploring patient-specific responses to viro-immunotherapy in glioblastoma, *Cells Rep. Methods*, 2024, **4**(3), 100716.

5 Y. Xie, T. Bergström, Y. Jiang, P. Johansson, V. D. Marinescu and N. Lindberg, *et al.*, The human glioblastoma cell culture resource: validated cell models representing all molecular subtypes, *EBioMedicine.*, 2015, **2**(10), 1351–1363.

6 A. Linkous, D. Balamatsias, M. Snuderl, L. Edwards, K. Miyaguchi and T. Milner, *et al.*, Modeling Patient-Derived Glioblastoma with Cerebral Organoids, *Cell Rep.*, 2019, **26**(12), 3203–3211.e5.

7 F. Jacob, R. D. Salinas, D. Y. Zhang, P. T. T. Nguyen, J. G. Schnoll and S. Z. H. Wong, *et al.*, A Patient-Derived Glioblastoma Organoid Model and Biobank Recapitulates Inter- and Intra-tumoral Heterogeneity, *Cell*, 2020, **180**(1), 188–204.e22.

8 F. Watanabe, E. W. Hollingsworth, J. M. Bartley, L. Wisehart, R. Desai and A. M. Hartlaub, *et al.*, Patient-derived organoids recapitulate glioma-intrinsic immune program and progenitor populations of glioblastoma, *PNAS Nexus*, 2024, **3**(2), pgae051.

9 V. G. LeBlanc, D. L. Trinh, S. Aslanpour, M. Hughes, D. Livingstone and D. Jin, *et al.*, Single-cell landscapes of primary glioblastomas and matched explants and cell lines show variable retention of inter- and intratumor heterogeneity, *Cancer Cell*, 2022, **40**(4), 379–392.e9.

10 L. F. Horowitz, A. D. Rodriguez, Z. Dereli-Korkut, R. Lin, K. Castro and A. M. Mikheev, *et al.*, Multiplexed drug testing of tumor slices using a microfluidic platform, *npj Precis. Oncol.*, 2020, **4**, 12.

11 K. Rambani, J. Vukasinovic, A. Glezer and S. M. Potter, Culturing thick brain slices: an interstitial 3D microperfusion system for enhanced viability, *J. Neurosci. Methods*, 2009, **180**(2), 243–254.

12 N. J. Killian, V. N. Vernekar, S. M. Potter and J. Vukasinovic, A Device for Long-Term Perfusion, Imaging, and Electrical Interfacing of Brain Tissue In vitro, *Front. Neurosci.*, 2016, **10**, 135.

13 Z. Liu, A. Mela, M. G. Argenziano, M. A. Banu, J. Furnari and C. Kotidis, *et al.*, Single-cell analysis of 5-aminolevulinic acid intraoperative labeling specificity for glioblastoma, *J. Neurosurg.*, 2024, **140**(4), 968–978.

14 Y. L. Cheng, M. A. Banu, W. Zhao, S. S. Rosenfeld, P. Canoll and P. A. Sims, Multiplexed single-cell lineage tracing of mitotic kinesin inhibitor resistance in glioblastoma, *Cell Rep.*, 2024, **43**(5), 114139.

15 O. Al-Dalahmah, M. G. Argenziano, A. Kannan, A. Mahajan, J. Furnari and F. Paryani, *et al.*, Re-convolving the compositional landscape of primary and recurrent glioblastoma reveals prognostic and targetable tissue states, *Nat. Commun.*, 2023, **14**(1), 2586.

16 M. A. Banu, A. Dovas, M. G. Argenziano, W. Zhao, C. P. Sperring and H. Cuervo Grajal, *et al.*, A cell state-specific metabolic vulnerability to GPX4-dependent ferroptosis in glioblastoma, *EMBO J.*, 2024, **43**(20), 4492–4521.

17 E. Tkachenko, E. Gutierrez, M. H. Ginsberg and A. Groisman, An easy to assemble microfluidic perfusion device with a magnetic clamp, *Lab Chip*, 2009, **9**(8), 1085–1095.

18 M. Halwes, M. Stamp and D. J. Collins, A Rapid Prototyping Approach for Multi-Material, Reversibly Sealed Microfluidics, *Micromachines*, 2023, **14**(12), 2213.

19 N. S. H. Motlagh, P. Parvin, F. Ghasemi and F. Atyabi, Fluorescence properties of several chemotherapy drugs: doxorubicin, paclitaxel and bleomycin, *Biomed. Opt. Express*, 2016, **7**(6), 2400–2406.

20 Z.-J. Chen, G. T. Gillies, W. C. Broaddus, S. S. Prabhu, H. Fillmore and R. M. Mitchell, *et al.*, A realistic brain tissue phantom for intraparenchymal infusion studies, *J. Neurosurg.*, 2004, **101**(2), 314–322.

21 H. Sjöberg, S. Persson and N. Caram-Lelham, How interactions between drugs and agarose-carrageenan hydrogels influence the simultaneous transport of drugs, *J. Controlled Release*, 1999, **59**(3), 391–400.

22 C. Lu, T. Kang, J. Zhang, K. Yang, Y. Liu and K. Song, *et al.*, Combined targeting of glioblastoma stem cells of different cellular states disrupts malignant progression, *Nat. Commun.*, 2025, **16**(1), 2974.

23 I. Miller, M. Min, C. Yang, C. Tian, S. Gookin and D. Carter, *et al.*, Ki67 is a Graded Rather than a Binary Marker of Proliferation versus Quiescence, *Cell Rep.*, 2018, **24**(5), 1105–1112.e5.

24 S. Reuter, S. C. Gupta, M. M. Chaturvedi and B. B. Aggarwal, Oxidative stress, inflammation, and cancer: how are they linked?, *Free Radical Biol. Med.*, 2010, **49**(11), 1603–1616.
25 A. Jalota, M. Kumar, B. C. Das, A. K. Yadav, K. Chosdol and S. Sinha, A drug combination targeting hypoxia induced chemoresistance and stemness in glioma cells, *Oncotarget*, 2018, **9**(26), 18351–18366.
26 B. A. Teicher, Hypoxia and drug resistance, *Cancer Metastasis Rev.*, 1994, **13**(2), 139–168.
27 N. S. Aboelella, C. Brandle, T. Kim, Z.-C. Ding and G. Zhou, Oxidative stress in the tumor microenvironment and its relevance to cancer immunotherapy, *Cancers*, 2021, **13**(5), 986.
28 M. J. Iqbal, A. Kabeer, Z. Abbas, H. A. Siddiqui, D. Calina and J. Sharifi-Rad, *et al.*, Interplay of oxidative stress, cellular communication and signaling pathways in cancer, *Cell Commun. Signaling*, 2024, **22**(1), 7.
29 K. M. Yamada and E. Cukierman, Modeling tissue morphogenesis and cancer in 3D, *Cell*, 2007, **130**(4), 601–610.
30 H. Kasai, Analysis of a form of oxidative DNA damage, 8-hydroxy-2′-deoxyguanosine, as a marker of cellular oxidative stress during carcinogenesis, *Mutat. Res.*, 1997, **387**(3), 147–163.
31 X. Qing, D. Shi, X. Lv, B. Wang, S. Chen and Z. Shao, Prognostic significance of 8-hydroxy-2′-deoxyguanosine in solid tumors: a meta-analysis, *BMC Cancer*, 2019, **19**(1), 997.
32 C.-Y. Ock, E.-H. Kim, D. J. Choi, H. J. Lee, K.-B. Hahm and M. H. Chung, 8-Hydroxydeoxyguanosine: not mere biomarker for oxidative stress, but remedy for oxidative stress-implicated gastrointestinal diseases, *World J. Gastroenterol.*, 2012, **18**(4), 302–308.
33 A. Valavanidis, T. Vlachogianni and C. Fiotakis, 8-hydroxy-2′ -deoxyguanosine(8-OHdG): A critical biomarker of oxidative stress and carcinogenesis, *J. Environ. Sci. Health, Part C: Environ. Carcinog. Ecotoxicol. Rev.*, 2009, **27**(2), 120–139.
34 L. L. Wu, C. C. Chiou, P. Y. Chang and J. T. Wu, Urinary 8-OHdG: a marker of oxidative stress to DNA and a risk factor for cancer, atherosclerosis and diabetics, *Clin. Chim. Acta*, 2004, **339**(1–2), 1–9.
35 A. Gozdz, B. Wojtaś, P. Szpak, P. Szadkowska, T. Czernicki and A. Marchel, *et al.*, Preservation of the Hypoxic Transcriptome in Glioblastoma Patient-Derived Cell Lines Maintained at Lowered Oxygen Tension, *Cancers*, 2022, **14**(19), 4852.
36 J. H. Park and H. K. Lee, Current understanding of hypoxia in glioblastoma multiforme and its response to immunotherapy, *Cancers*, 2022, **14**(5), 1176.
37 S. Arfin, N. K. Jha, S. K. Jha, K. K. Kesari, J. Ruokolainen and S. Roychoudhury, *et al.*, Oxidative stress in cancer cell metabolism, *Antioxidants*, 2021, **10**(5), 642.
38 A. Muslimović, S. Nyström, Y. Gao and O. Hammarsten, Numerical analysis of etoposide induced DNA breaks, *PLoS One*, 2009, **4**(6), e5859.
39 A. Z. Mohammad, J. Sule Suso and N. Forsyth, Precision control of dissolved oxygen in mammalian cell culture media impacts on in situ volatile generation and promotes improved mesenchymal stem cell yield accompanied by reduced transcriptional variability, *Free Radical Biol. Med.*, 2015, **86**, S16.
40 D. Newby, L. Marks and F. Lyall, Dissolved oxygen concentration in culture medium: assumptions and pitfalls, *Placenta*, 2005, **26**(4), 353–357.
41 Y. Huang, J. C. Williams and S. M. Johnson, Brain Slice on a Chip: Opportunities and Challenges of Applying Microfluidic Technology to Intact Tissues, *Lab Chip*, 2012, **12**, 2103–2117.
42 A. Carreau, B. El Hafny-Rahbi, A. Matejuk, C. Grillon and C. Kieda, Why is the partial oxygen pressure of human tissues a crucial parameter? Small molecules and hypoxia, *J. Cell. Mol. Med.*, 2011, **15**(6), 1239–1253.
43 G. Mehta, K. Mehta, D. Sud, J. W. Song, T. Bersano-Begey and N. Futai, *et al.*, Quantitative measurement and control of oxygen levels in microfluidic poly(dimethylsiloxane) bioreactors during cell culture, *Biomed. Microdevices*, 2007, **9**(2), 123–134.
44 L. Ostergaard, A. Tietze, T. Nielsen, K. R. Drasbek, K. Mouridsen and S. N. Jespersen, *et al.*, The relationship between tumor blood flow, angiogenesis, tumor hypoxia, and aerobic glycolysis, *Cancer Res.*, 2013, **73**(18), 5618–5624.
45 J. P. Fisher and D. C. Adamson, Current FDA-Approved Therapies for High-Grade Malignant Gliomas, *Biomedicines*, 2021, **9**(3), 324.
46 L. Lei, A. M. Sonabend, P. Guarnieri, C. Soderquist, T. Ludwig and S. Rosenfeld, *et al.*, Glioblastoma models reveal the connection between adult glial progenitors and the proneural phenotype, *PLoS One*, 2011, **6**(5), e20041.
47 J. Yuan and P. A. Sims, An Automated Microwell Platform for Large-Scale Single Cell RNA-Seq, *Sci. Rep.*, 2016, **6**, 33883.
48 J. Yuan, H. M. Levitin, V. Frattini, E. C. Bush, D. M. Boyett and J. Samanamud, *et al.*, Single-cell transcriptome analysis of lineage diversity in high-grade glioma, *Genome Med.*, 2018, **10**(1), 57.
49 H. M. Levitin, J. Yuan, Y. L. Cheng, F. J. Ruiz, E. C. Bush and J. N. Bruce, *et al.*, De novo gene signature identification from single-cell RNA-seq with hierarchical Poisson factorization, *Mol. Syst. Biol.*, 2019, **15**(2), e8557.
50 J. A. Griffiths, A. C. Richard, K. Bach, A. T. L. Lun and J. C. Marioni, Detection and removal of barcode swapping in single-cell RNA-seq data, *Nat. Commun.*, 2018, **9**(1), 2667.
51 A. T. L. Lun, S. Riesenfeld, T. Andrews, T. P. Dao, T. Gomes and participants in the 1st Human Cell Atlas Jamboree, *et al.*, EmptyDrops: distinguishing cells from empty droplets in droplet-based single-cell RNA sequencing data, *Genome Biol.*, 2019, **20**(1), 63.
52 P. A. Szabo, H. M. Levitin, M. Miron, M. E. Snyder, T. Senda and J. Yuan, *et al.*, Single-cell transcriptomics of human T cells reveals tissue and activation signatures in health and disease, *Nat. Commun.*, 2019, **10**(1), 4706.
53 A. T. L. Lun, K. Bach and J. C. Marioni, Pooling across cells to normalize single-cell RNA sequencing data with many zero counts, *Genome Biol.*, 2016, **17**, 75.
54 E. E. Bar, A. Lin, V. Mahairaki, W. Matsui and C. G. Eberhart, Hypoxia increases the expression of stem-cell markers and promotes clonogenicity in glioblastoma neurospheres, *Am. J. Pathol.*, 2010, **177**(3), 1491–1502.
55 I. C. McLean, L. A. Schwerdtfeger, S. A. Tobet and C. S. Henry, *Lab Chip*, 2018, **18**(10), 1399–1410.

56 P. M. van Midwoud, M. T. Merema, E. Verpoorte and G. M. Groothuis, A microfluidic approach for in vitro assessment of interorgan interactions in drug metabolism using intestinal and liver slices, *Lab Chip*, 2010, **10**(20), 2778–2786.
57 S. Shim, M. C. Belanger, A. R. Harris, J. M. Munson and R. R. Pompano, Two-way communication between ex vivo tissues on a microfluidic chip: application to tumor-lymph node interaction, *Lab Chip*, 2019, **19**(6), 1013–1026.
58 M. Astolfi, B. Péant, M. A. Lateef, N. Rousset, J. Kendall-Dupont, E. Carmona, F. Monet, F. Saad, D. Provencher, A. M. Mes-Masson and T. Gervais, Micro-dissected tumor tissues on chip: an ex vivo method for drug testing and personalized therapy, *Lab Chip*, 2016, **16**(2), 312–325.
59 L. F. Horowitz, A. D. Rodriguez, A. Au-Yeung, K. W. Bishop, L. A. Barner, G. Mishra, A. Raman, P. Delgado, J. T. C. Liu, T. S. Gujral, M. Mehrabi, M. Yang, R. H. Pierce and A. Folch, Microdissected "cuboids" for microfluidic drug testing of intact tissues, *Lab Chip*, 2021, **21**(1), 122–142.
60 J. A. Rey, J. R. Ewing and M. Sarntinoranont, A computational model of glioma reveals opposing, stiffness-sensitive effects of leaky vasculature and tumor growth on tissue mechanical stress and porosity, *Biomech. Model. Mechanobiol.*, 2021, **20**(5), 1981–2000, DOI: 10.1007/s10237-021-01488-8.
61 S. R. McKeown, Defining normoxia, physoxia and hypoxia in tumours-implications for treatment response, *Br. J. Radiol.*, 2014, **87**(1035), 20130676.
62 J. Grote, R. Süsskind and P. Vaupel, Oxygen diffusivity in tumor tissue(DS-carcinosarcoma) under temperature conditions within the range of 20–40 degrees C, *Pflugers Arch*, 1977, **372**(1), 37–42.
63 A. J. McGoron, P. Nair and R. W. Schubert, Michaelis-Menten kinetics model of oxygen consumption by rat brain slices following hypoxia, *Ann. Biomed. Eng.*, 1997, **25**(3), 565–572.
64 K. Groebe and W. Mueller-Klieser, Distributions of oxygen, nutrient, and metabolic waste concentrations in multicellular spheroids and their dependence on spheroid parameters, *Eur. Biophys. J.*, 1991, **19**(4), 169–181.